Abdominal Imaging

Published online: 30 April 2008

Abdom Imaging (2009) 34:391–402
DOI: 10.1007/s00261-008-9405-7

Imaging of peritoneal carcinomatosis with FDG PET-CT: diagnostic patterns, case examples and pitfalls

Anna Maria DeGaetano, Maria Lucia Calcagni, Vittoria Rufini, Venanzio Valenza, Alessandro Giordano, Lorenzo Bonomo

Department of Bioimaging and Radiological Sciences, Catholic University of the Sacred Heart, Agostino Gemelli Hospital, Largo Agostino Gemelli 8, Rome 00168, Italy

Abstract

Early diagnosis of peritoneal spread in malignant disease is essential to prevent unnecessary laparotomies and to select the patients in whom complete cytoreduction is feasible. Although anatomic imaging is the mainstay for evaluating peritoneal seeding, small neoplastic implants can be difficult to detect with CT and MR imaging. FDG PET-CT has the potential to improve detection of peritoneal metastases as lesion conspicuity is high at PET due to low background activity and fused PET-CT offers the combined benefits of anatomic and functional imaging. Correlation of uptake modalities with the pathogenesis of intraperitoneal spread of malignancies, provides a rational system of analysis and is essential to define disease. Distinct patterns appear to predict the presence of either nodular or diffuse peritoneal pathology. Main pitfalls are related to normal physiologic activity in bowel loops and blood vessels or focal retained activity in ureters and urinary bladder. PET-CT is most suitable in patients with high tumor markers and negative or uncertain conventional imaging data and in selecting patients for complete cytoreduction. FDG PET-CT adds to conventional imaging in the detection and staging of peritoneal carcinomatosis and is a useful diagnostic tool in monitoring response to therapy and in long term follow-up.

Key words: FDG PET-CT—Peritoneal carcinomatosis—Peritoneum—Ovarian cancer—Cancer diagnosis

Correspondence to: Anna Maria DeGaetano; *email:* adegaetano@rm.unicatt.it

Early diagnosis of peritoneal spread in malignant disease is essential to prevent unnecessary laparotomies and to select the patients in whom complete cytoreduction is feasible [1, 2].

Although anatomic imaging is the mainstay for evaluating peritoneal seeding, small neoplastic implants can be difficult to detect with CT and MR imaging [3–7]. 2-[Fluorine 18] fluoro-2-deoxy-D-glucose (FDG) positron emission tomography (PET) detects increased glucose metabolism associated with neoplastic lesions and provides high accuracy in most cancer imaging applications [8, 9]. The recent development and use of hybrid PET-CT scanners allows functional and anatomic data to be obtained in a single examination, improving lesion localization and resulting in significant diagnostic improvement [10–14].

At PET-CT peritoneal implants appear as nodular soft tissue masses, with increased activity; neoplastic nodules can coalesce in larger masses and coat abdominal viscera [15–17]. Distinct patterns appear to predict the presence of either nodular or diffuse peritoneal pathology (Fig. 1) [18].

Correlation of uptake modalities with the pathogenesis of peritoneal carcinomatosis provides a rational system of analysis and is essential to define disease. The spread of neoplasms within the peritoneal cavity can occur by intraperitoneal seeding. A primary neoplasm, in breaking through into the peritoneal cavity can shed cells into the ascitic fluid induced [19]. The intraperitoneal fluid continually follows a circulation through the abdomen allowing transportation and deposition of malignant cells. Dynamic pathways of spread depend on anatomic features, forces of gravity, and negative subdiaphragmatic pressure [20].

The peritoneal cavity is subdivided by peritoneal reflections and mesenteric attachments into compartments and recesses (Fig. 2) creating an interconnecting

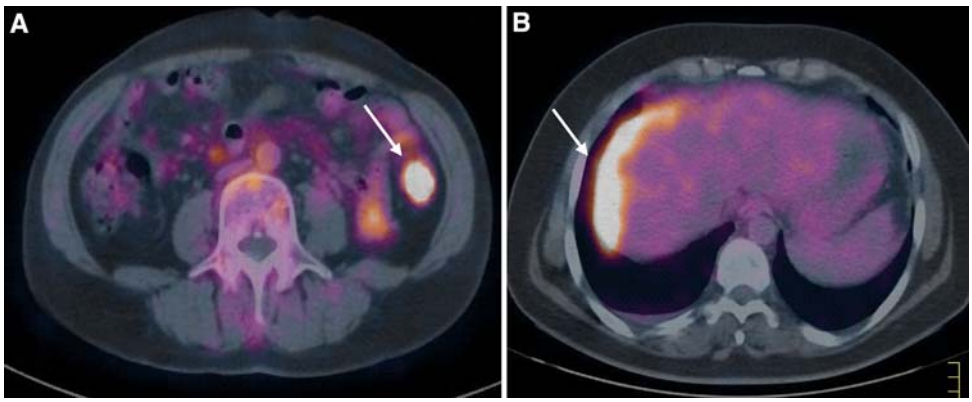

Fig. 1. PET-CT patterns of peritoneal implants. (**A**) Nodular pattern: fused PET-CT transverse scan shows a focal area of intense FDG uptake in the left paracolic gutter (*arrow*). (**B**) Diffuse pattern: fused PET-CT transverse scan shows diffuse thickening and intense uptake of the liver capsule (*arrow*).

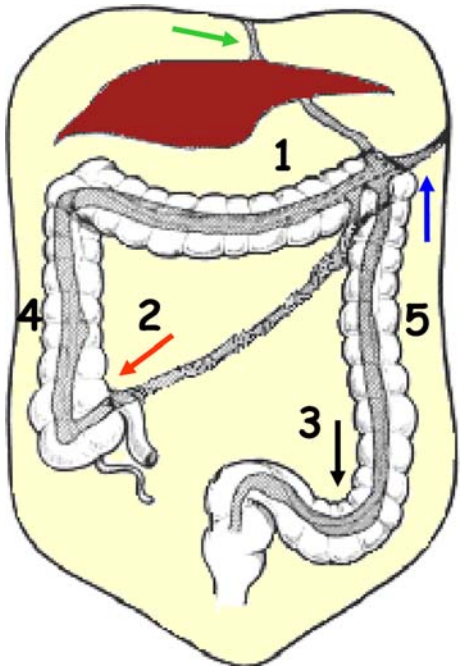

Fig. 2. Anatomic features of the peritoneal cavity. The transverse mesocolon divides the abdominal cavity into the supramesocolic (1) and inframesocolic spaces. The small bowel mesentery divides the inframesocolic space into two comparments, the right (2) and left (3) infracolic spaces. The right (4) and left (5) paracolic gutters are lateral to the attachments of the peritoneal reflections of the ascending and descending colon. The right infracolic space terminates at the junction of cecum and terminal ileum (*red arrow*). The left infracolic space opens anatomically to the pelvis to the right of the midline and toward the left it is restricted from continuity with the pelvic cavity by the sigmoid mesocolon (*black arrow*). The right and left paracolic gutters represent communications between the lower abdomen and pelvis with the supramesocolic area. On the left the phrenicocolic ligament partially separates the paracolic gutter from the perisplenic space (*blue arrow*). The falciform ligament separates the right from the left subphrenic space (*green arrow*) (Modified from Meyers MA: The spread and localization of acute intraperitoneal effusions. Radiology 1970; 95:547–554).

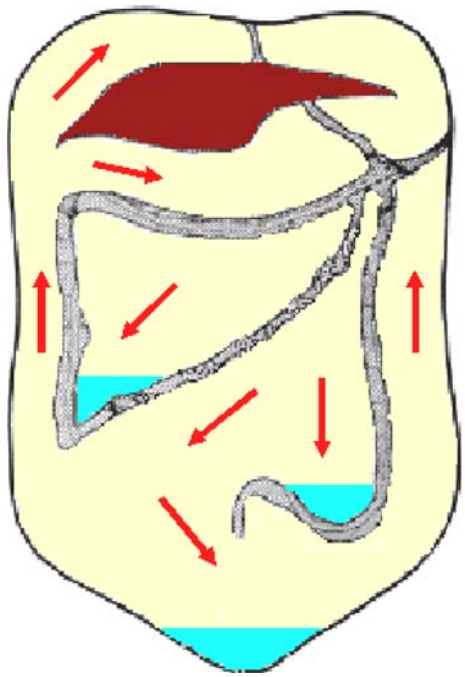

Fig. 3. Pathways of ascitic fluid and sites of pooling and seeding. The force of gravity operates to pool peritoneal fluid in pelvic recesses while negative subdiaphragmatic pressure directs fluid upward along paracolic gutters. From the right infracolic space fluid pools at the ileo-cecal junction while from the left infracolic space it pools at the sigmoid mesocolon and then overflows into the pelvis. From the pelvis, fluid ascends the right paracolic gutter to the right subhepatic and subphrenic spaces. The falciform ligament prevents diffusion to the left subphrenic space. Passage along the shallower left paracolic gutter is slow and weak and limited cephalad by the phrenicocolic ligament (Modified from Meyers MA: The spread and localization of acute intraperitoneal effusions. Radiology 1970; 95:547–554).

network [21, 22]. The transverse mesocolon, small bowel mesentery, sigmoid mesocolon, and the peritoneal attachments of the ascending and descending colon serve

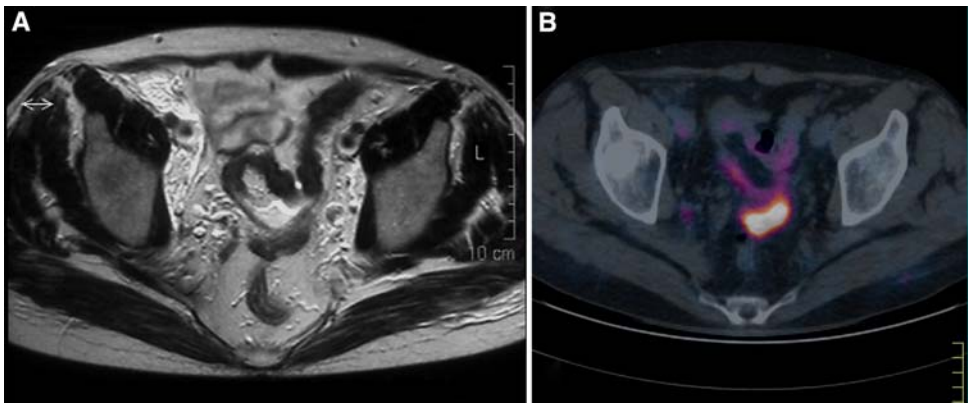

Fig. 4. Neoplastic involvement of the pelvic peritoneum. (**A**) Transverse T2 weighted fast spin-echo MR image shows peritoneal thickening and a small amount of ascites in the pouch of Douglas. (**B**) Fused PET-CT transverse scan shows diffuse intense FDG uptake in the pouch of Douglas.

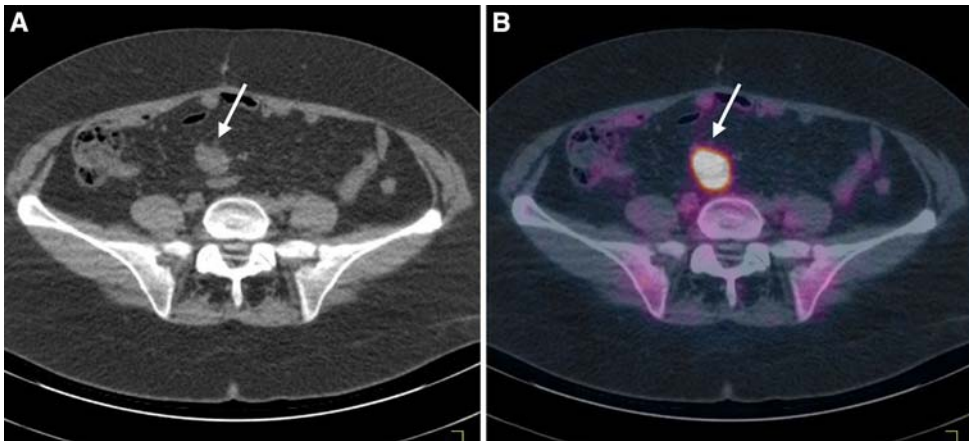

Fig. 5. Mesenteric neoplastic nodule. (**A**) Low dose CT shows a soft tissue nodule in the small bowel mesentery (*arrow*). (**B**) Fused PET CT axial scan shows a focal area of intense FDG uptake corresponding to the tumor nodule. (*arrow*).

as watershed directing the flow of ascites. Pooling of peritoneal fluid favors deposition, fixation, and growth of seeded malignant cells [19, 20]. The force of gravity operates to pool peritoneal fluid in depended pelvic recesses while negative subdiaphragmatic pressure directs fluid upward along paracolic gutters. From the right infracolic space, fluid pools at the ileo-cecal junction, and then overflows into the pelvis. From the left infracolic space fluid pools at the sigmoid mesocolon and then channels into the pelvis. From the pelvis fluid ascends the right paracolic gutter to the right subhepatic and subphrenic spaces. The falciform ligament prevents diffusion to the left subphrenic space. Passage through the shallower left paracolic gutter is slow and weak and limited cephalad by the phrenicocolic ligament (Fig. 3) [19, 20].

The main sites of growth of seeded metastasis follow the pathways of ascitic flow and are: the pouch of Douglas, the small bowel mesentery, the ileo-cecal junction, the right and left paracolic gutters, the hepatorenal fossa, and the right subphrenic space [19, 20].

The pouch of Douglas is the most dependent portion of the peritoneal cavity and is involved in over 50% of cases (Fig. 4) [19, 20].

Small bowel mesentery is involved in over 40% of cases. Pooling in peritoneal recesses of mesenteric ruffles favors seeding of malignant cells on mesenteric borders of ileal loops and spread occurs from one mesenteric ruffle to the other, along the axis if the small bowel mesentery, toward the ileo-cecal junction and the pelvis (Fig. 5) [19, 20, 23].

The sigmoid mesocolon is involved in about 20% of cases as from the left infracolic space fluid pools along the superior border of the sigmoid colon (Fig. 6) [19, 20].

The right paracolic gutter is involved in about 18% of cases as the major flow from the pelvis is up the right paracolic gutter and neoplastic implants can, therefore, occur along the cecum and ascending colon (Fig. 7) [19, 20].

Neoplastic implants can also occur along the left paracolic gutter although flow up the shallower left paracolic gutter is slow and weak and cephalad extension is limited by the phrenicocolic ligament (Fig. 8) [19, 20].

Neoplastic implants are also seen in the hepatorenal fossa (Morison's pouch) as in the supine position, it is the lowest part of the right paravertebral groove and communicates with the right subphrenic space and the right paracolic gutter (Fig. 9) [24].

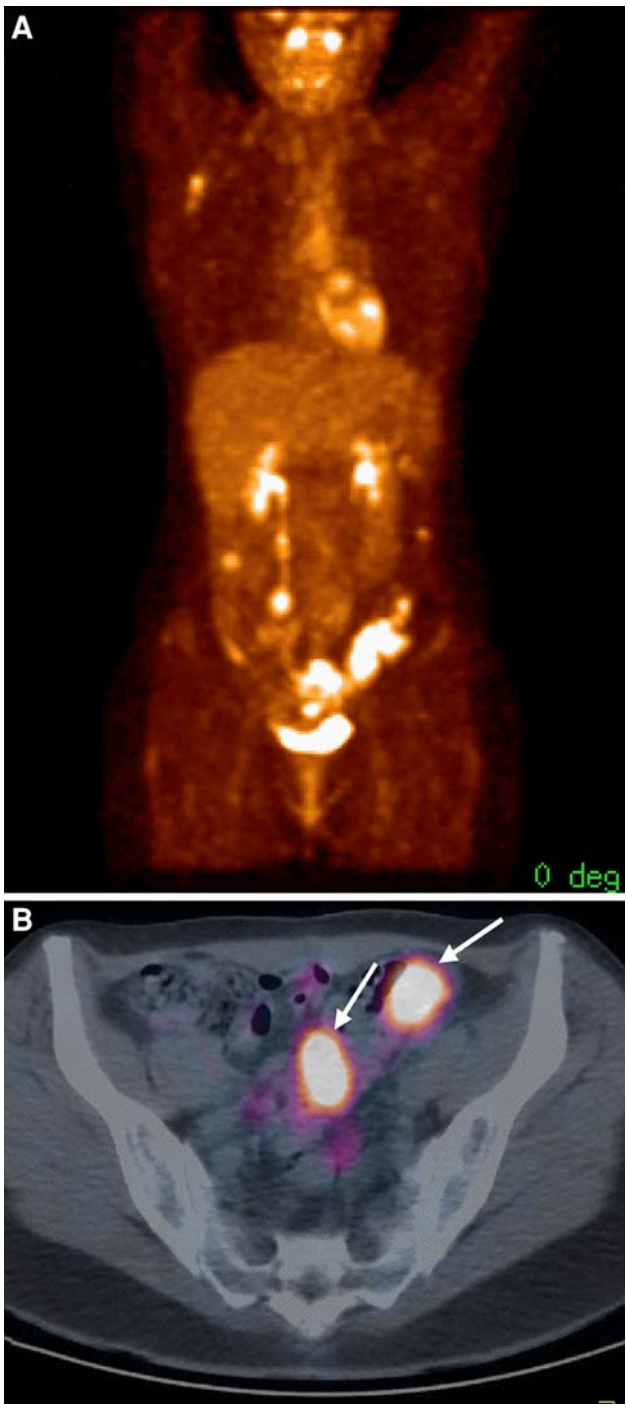

Fig. 6. Peritoneal carcinomatosis with neoplastic nodules along the superior border of the sigmoid colon. (**A**) Maximum-intensity projection FDG PET image shows multiple areas of increased uptake in the abdomen and pelvis, preferentially located in the left iliac fossa. Hypermetabolic lymph nodes are also present in the right axilla. (**B**) Axial fused PET CT image shows focal areas of intense FDG uptake along the sigmoid colon (*arrows*).

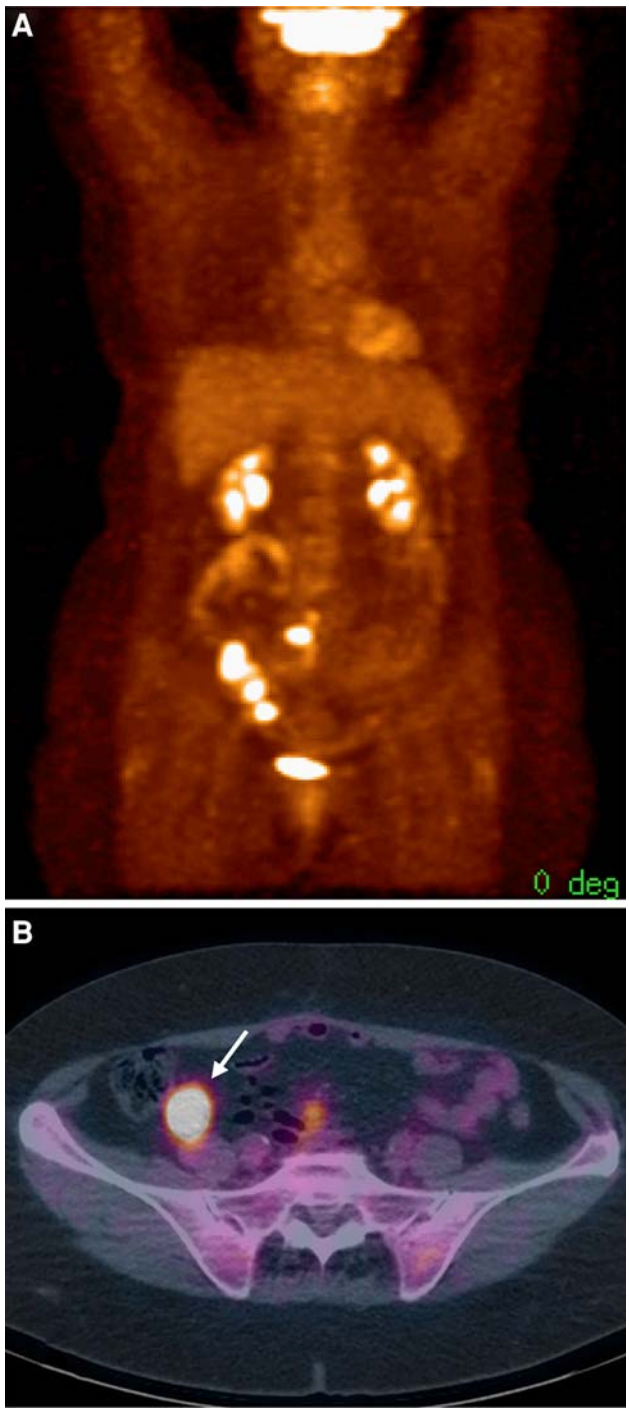

Fig. 7. Peritoneal carcinomatosis with neoplastic nodules along the cecum and ascending colon. (**A**) Maximum-intensity projection FDG PET image shows areas of increased uptake in the right iliac fossa and lower abdomen. (**B**) Axial fused PET CT image shows a pericecal nodular area of intense FDG uptake (*arrow*).

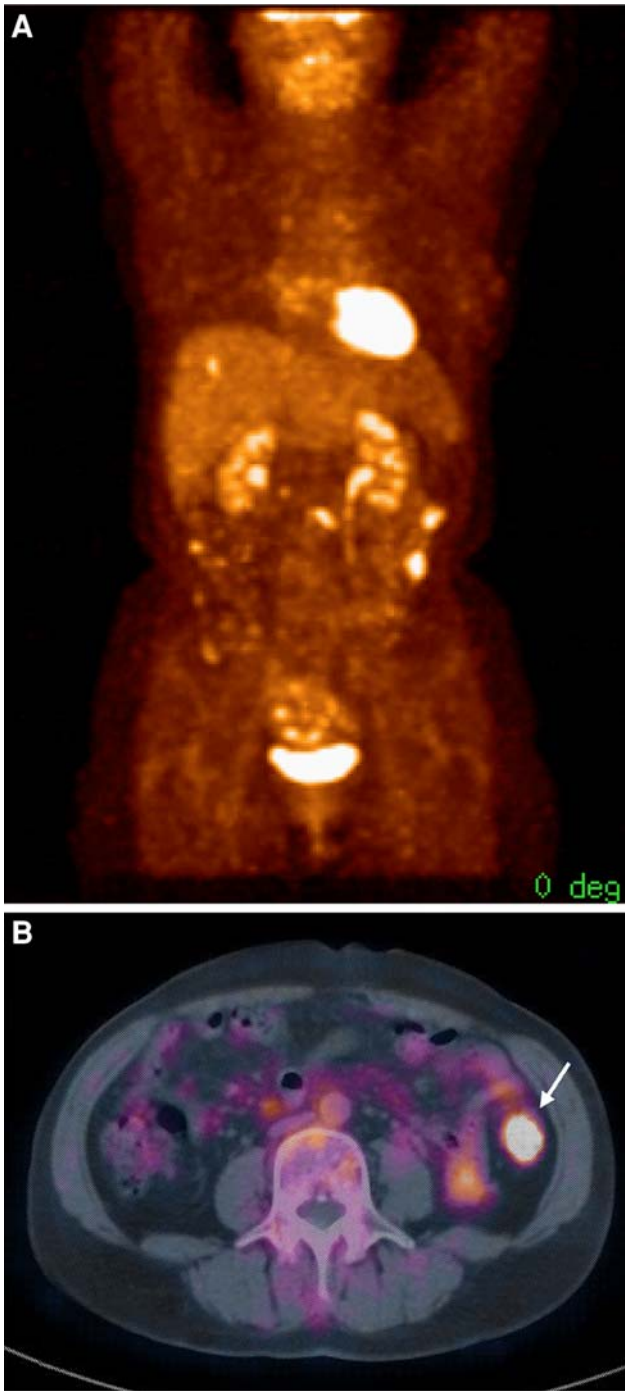

Fig. 8. Peritoneal carcinomatosis with neoplastic nodules in the left paracolic gutter. (**A**) Maximum-intensity projection FDG PET image shows areas of increased uptake in the abdomen, liver capsule, and pelvis. The left paracolic gutter is also involved. (**B**) Axial fused PET CT image shows an hypermetabolic nodule in the left paracolic gutter (*arrow*).

Implants in the right subphrenic space, along the right hemidiaphragm and liver capsule are frequent. The falciform ligament is a relevant site of implantation and prevents diffusion to the left subphrenic space (Fig. 10) [19–21].

From the abdomen tumor can spread to the right hemithorax owing to connections between the right subphrenic space and the right pleura through the diaphragm (Fig. 11).

The greater omentum is rich in lymphoid tissue, absorbs peritoneal fluid and is a frequent site of neoplastic seeding [19]. In omental involvement, PET-CT shows omental thickening, hyperdensity, and nodularity, with high and diffuse FDG uptake (Fig. 12) [25].

Umbilical neoplastic nodules, called Sister Mary Joseph's nodules, are localized in the anterior abdominal wall and are sign of abdominal spread of malignancy (Fig. 13) [26].

FDG PET-CT adds to conventional imaging in diagnosis and staging of peritoneal carcinomatosis as this technique can detect lesions not identified by CT (Fig. 14) [14–18]. FDG PET-CT can also detect lesions misdiagnosed, because of their unusual location (Fig. 15) or their small size (Fig. 16). In mixed solid and cystic lesions uptake is seen in the solid component but not in the fluid portion (Figs. 17 and 18).

Neoplastic peritoneal or mesenteric masses can involve adjacent bowel loops resulting in bowel obstruction (Fig. 19). Neoplastic spread in the peritoneal cavity frequently causes ascites. The presence of ascites allows differentiation of neoplastic implants over the visceral or the parietal peritoneum (Figs. 20 and 21). PET-CT false negative results are related to cystic lesions, (Fig. 22) small volume disease or miliaric peritoneal involvement. False positive diagnoses seem mainly related to bowel activity or focal retained activity in ureters and urinary bladder (Fig. 23) [27].

FGD PET-CT has the potential to improve detection of peritoneal carcinomatosis as lesion conspicuity is high at PET due to low background activity.

Knowledge of anatomic features of the peritoneal cavity and of the pathogenesis of intraperitoneal spread of malignancies are essential to properly locate and define disease. FDG-PET allows for an improved decision-making process regarding treatment with surgery or chemotherapy. It can also be used for monitoring response to therapy (Fig. 24) and in long term follow-up.

References

1. Al-Shammaa HA, Li Y, Yonemura Y (2008) Current status and future strategies of cytoreductive surgery plus intraperitoneal hyperthermic chemotherapy for peritoneal carcinomatosis. World J Gastroenterol 14(8):1159–1166
2. Gusani NJ, Cho SW, Colovos C, et al. (2008) Aggressive surgical management of peritoneal carcinomatosis with low mortality in a high-volume tertiary cancer center. Ann Surg Oncol 15(3):754–763
3. Forstner R, Hricak H, Occhipinti KA, et al. (1995) Ovarian cancer: staging with CT and MR imaging. Radiology 197(3):619–626
4. Forstner R, Hricak H, Powell CB, et al. (1995) Ovarian cancer recurrence: value of MR imaging. Radiology 196(3):715–720
5. Forstner R (2007) Radiological staging of ovarian cancer: imaging findings and contribution of CT and MRI. Eur Radiol 17(12):3223–3235

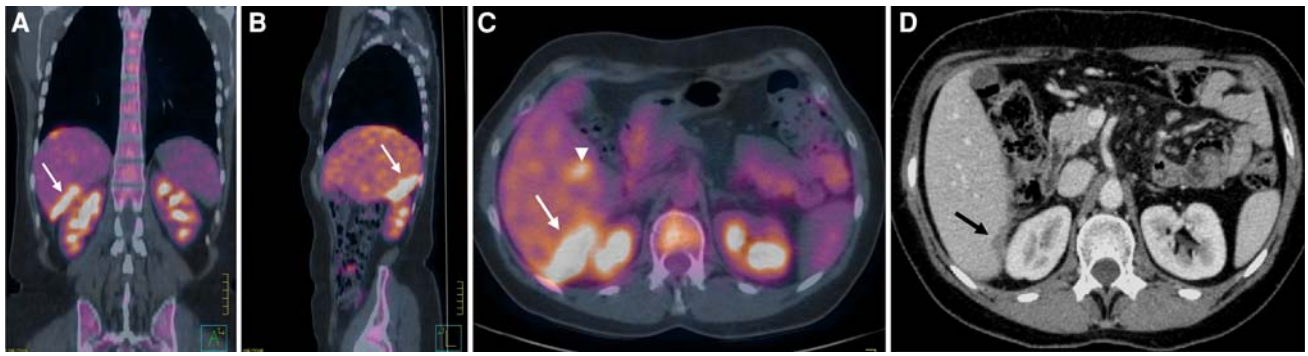

Fig. 9. Peritoneal carcinomatosis with involvement of Morison's pouch. Coronal (**A**), sagittal (**B**), and axial (**C**) fused PET CT images show hypermetabolic tissue along the liver capsule in Morison's pouch (*arrows*). In (**C**) a focal area of intense FDG uptake is also seen in a liver fessure (*arrowhead*). (**D**) Contrast-enhanced CT shows plaquelike thickening of the liver capsule at Morison's pouch (*arrow*).

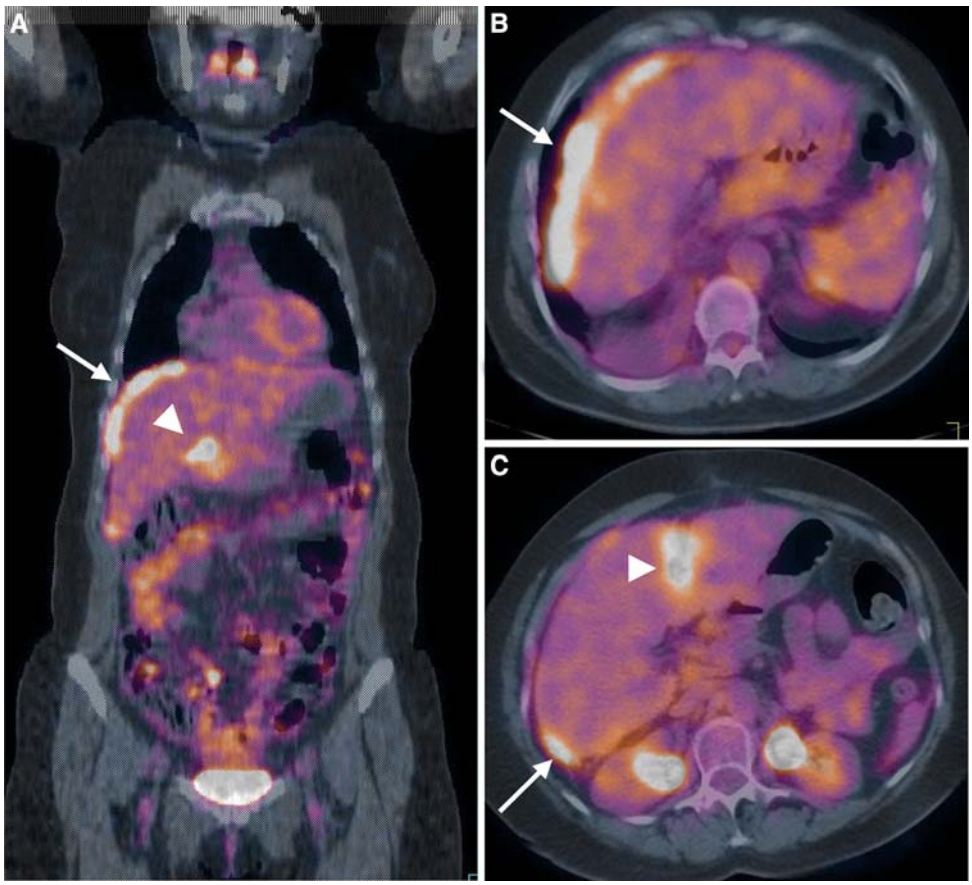

Fig. 10. Peritoneal carcinomatosis with implants along the liver capsule and the falciform ligament. Coronal (**A**) and axial (**B**) and (**C**) fused PET CT images show hypermetabolic tissue along the liver capsule in the right subphrenic space (*arrows*). Involvement of the falciform ligament is also present (*arrowheads*).

6. Coakley FV, Choi PH, Gougoutas CA, et al. (2002) Peritoneal metastases: detection with spiral CT in patients with ovarian cancer. Radiology 223(2):495–499
7. Kubik-Huch RA, Dörffler W, von Schulthess GK, et al. (2000) Value of (18F)-FDG positron emission tomography, computed tomography, and magnetic resonance imaging in diagnosing primary and recurrent ovarian carcinoma. Eur Radiol 10(5):761–767
8. Rohren EM, Turkington TG, Coleman RE (2004) Clinical Applications of PET in Oncology. Radiology 231:305–332
9. Zimny M, Siggelkow W, Schroder W, et al. (2001) 2-[Fluorine-18]-fluoro-2-deoxy-d-glucose positron emission tomography in the diagnosis of recurrent ovarian cancer. Gynecol Oncol 83(2):310–315
10. von Schulthess GK, Steinert HC, Hany TF (2006) Integrated PET/CT: current applications and future directions. Radiology 238:405–422
11. Kapoor V, McCook BM, Torok FS (2004) An introduction to PET-CT imaging. Radiographics 24(2):523–543

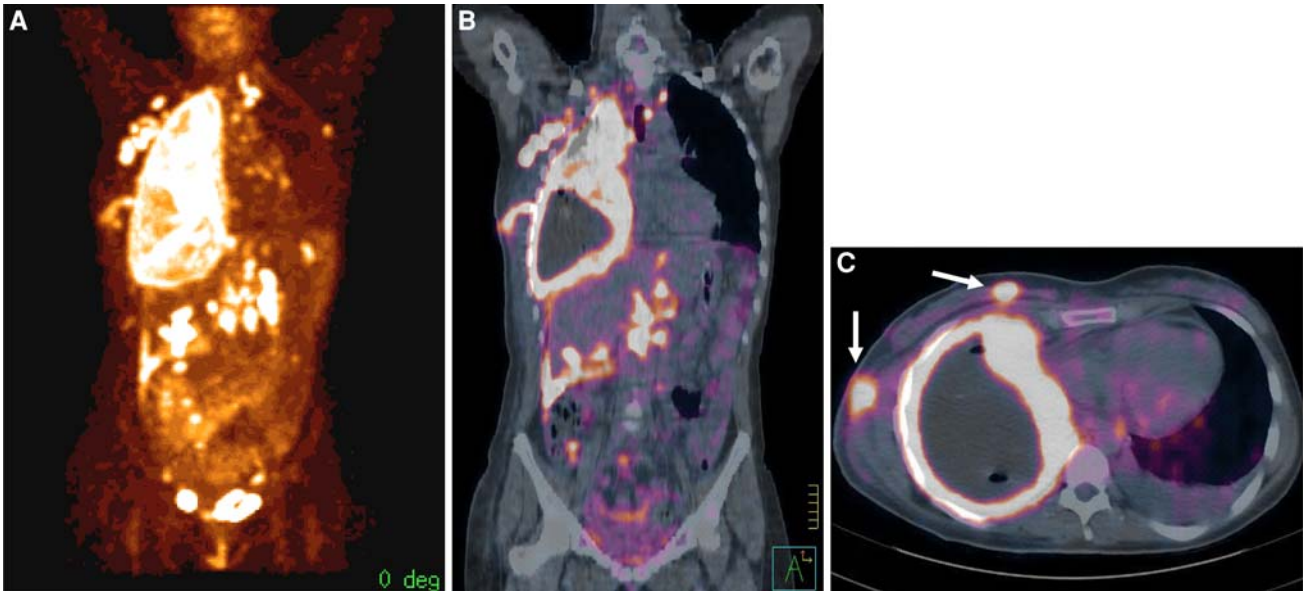

Fig. 11. Peritoneal carcinomatosis with tumor spread to the right hemithorax. (**A**) Maximum-intensity projection FDG PET image shows multiple areas of increased uptake in the abdomen, pelvis, and right hemithorax. Hypermetabolic lymph nodes are present in the mediastinum and in both axillae. (**B**) Coronal fused PET CT image shows multiple perihepatic areas of high FDG uptake. Massive involvement of the right pleura is seen with a fluid collection. Hypermetabolic lymph nodes are shown in the mediastinum and in the right axilla. Parietal nodules with high uptake are present in the right thoracic wall. (**C**) Axial fused PET CT image confirms right pleural neoplastic involvement with parietal nodules (*arrows*). Left pleural effusion is also shown.

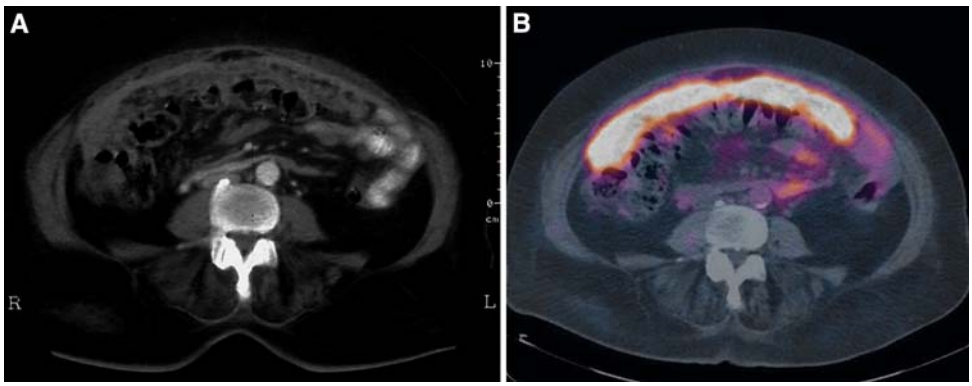

Fig. 12. Neoplastic involvement of the greater omentum. (**A**) Contrast-enhanced CT shows omental caking and enhancement of tumor implants. (**B**) Fused PET CT axial scan shows diffuse and high FDG uptake of the greater omentum.

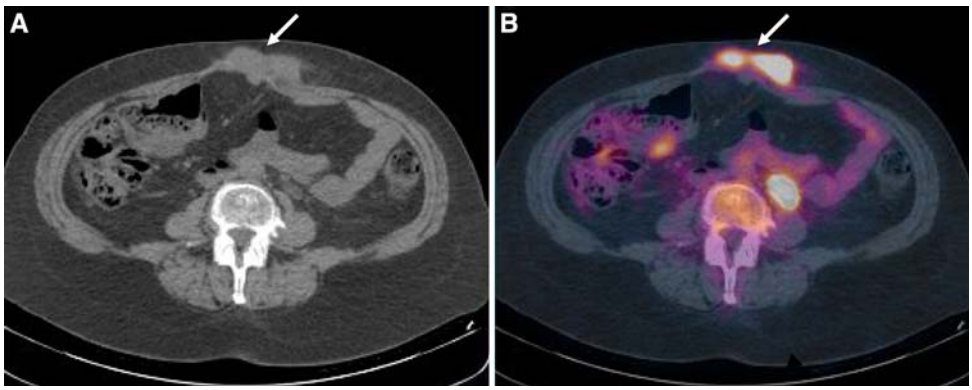

Fig. 13. Sister Mary Joseph's nodules. (**A**) Low dose CT shows subcutaneous umbilical nodules (*arrow*). (**B**) Fused PET CT axial scan shows intense FDG uptake of the umbilical implants (*arrow*).

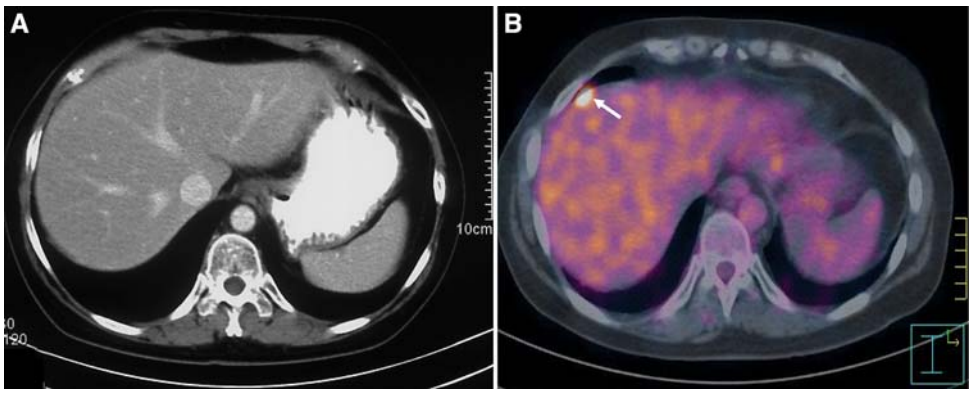

Fig. 14. Neoplastic implant on the liver capsule not detected by CT. (**A**) Contrast-enhanced CT does not detect any liver lesion. (**B**) Axial fused PET CT scan shows a hypermetabolic lesion on the liver capsule (*arrow*).

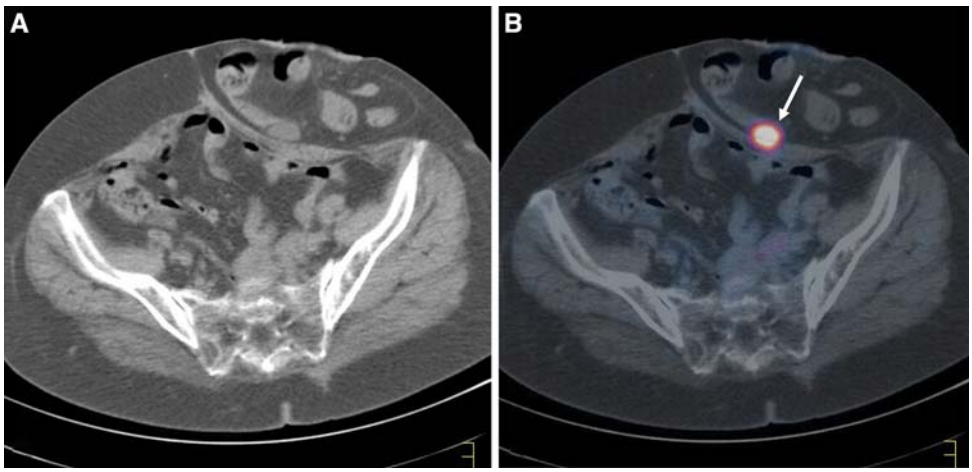

Fig. 15. Neoplastic implant misdiagnosed by CT in a patient with laparocele. (**A**) At contrast-enhanced CT no neoplastic lesion was reported. Low dose axial scan shows left laparocele with ileal loops herniation. (**B**) Axial fused PET CT scan shows a hypermetabolic nodule in the adipose tissue of the hernial sac (*arrow*).

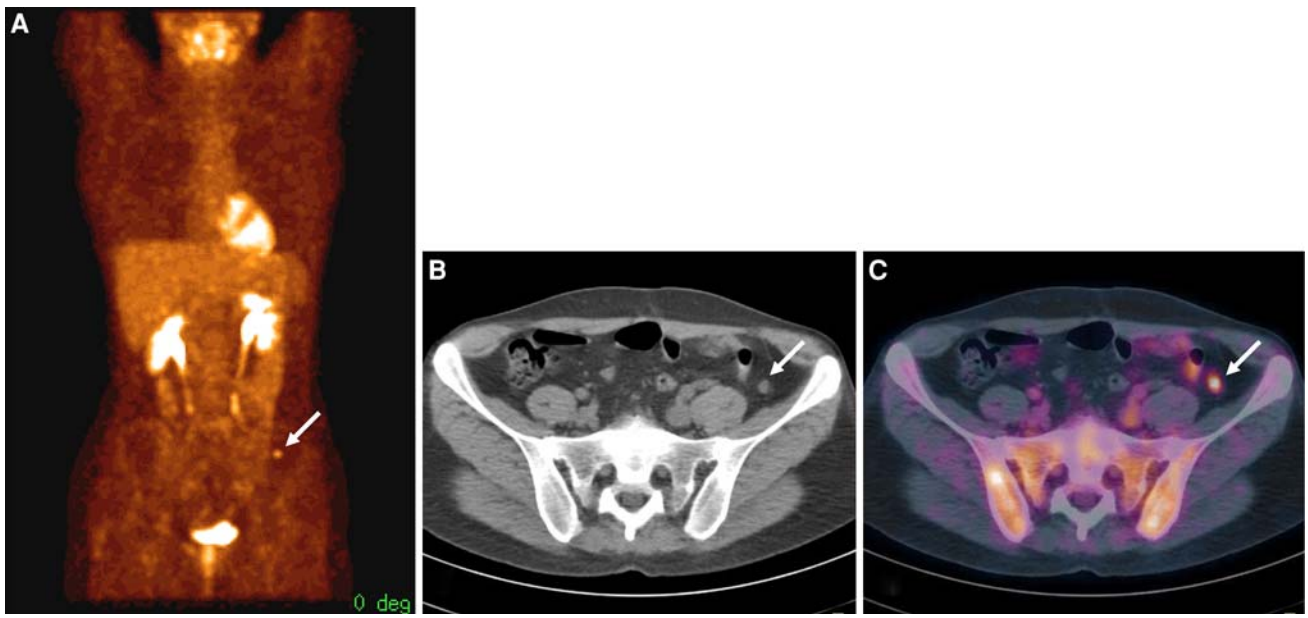

Fig. 16. Small neoplastic implant misdiagnosed by CT in the left paracolic gutter. (**A**) Maximum-intensity projection FDG PET image shows a small area of increased uptake in the left iliac fossa (*arrow*). Low dose CT, (**B**) and axial fused PET CT scan (**C**) show a 1 cm. nodule with intense FDG uptake in the left paracolic gutter (*arrow*).

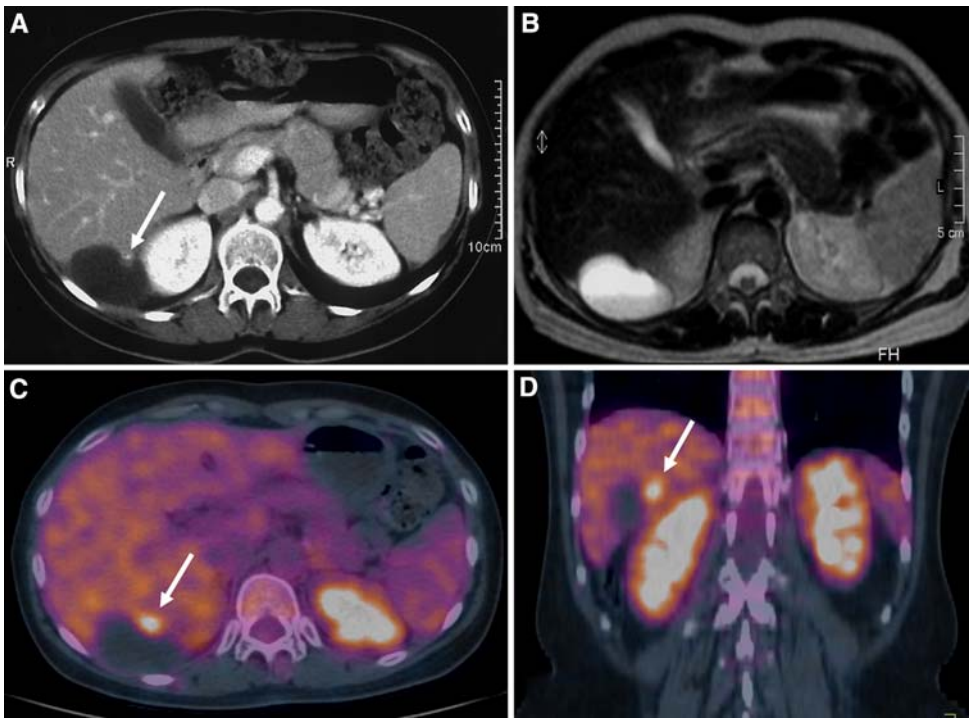

Fig. 17. Ovarian carcinoma—cystic peritoneal neoplastic implant. (**A**) Postcontrast CT scan shows a cystic lesion located posterior to the VI liver segment and lateral to the right kidney. A small nodular thickening of the anterior cystic wall is present (*arrow*). (**B**) T2 weighted fast spin-echo axial MR image confirms CT data and shows a fluid/fluid level. (**C**, **D**) Axial and coronal PET-CT fused scans show a focus of high FDG uptake in the nodular wall thickening (*arrows*). Surgery revealed ovarian carcinoma recurrence.

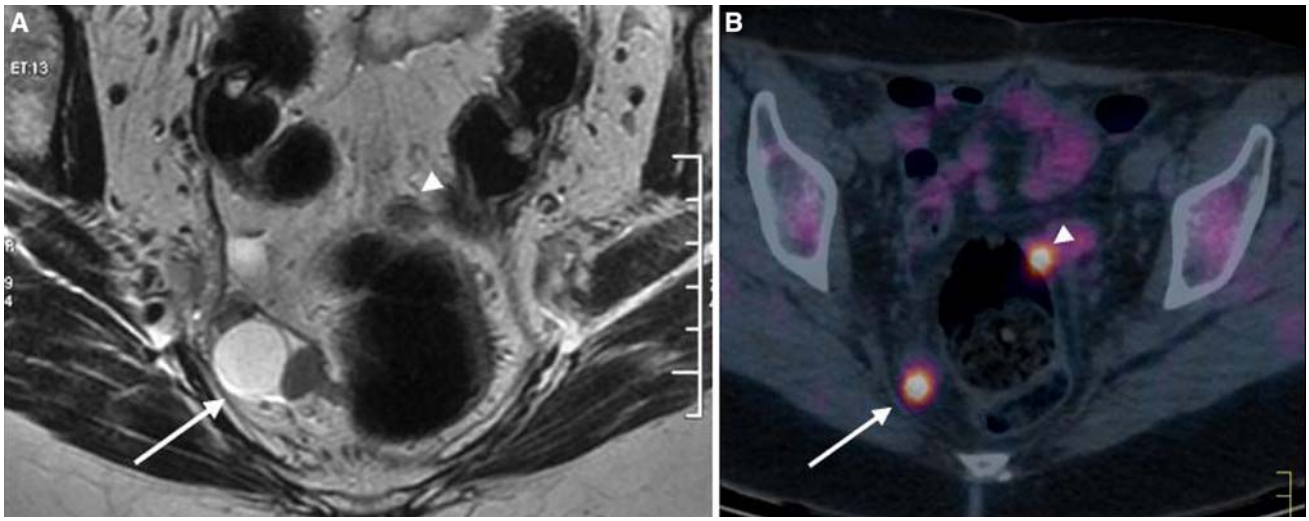

Fig. 18. Perirectal ovarian carcinoma neoplastic implants. (**A**) T2 weighted fast spin-echo transverse MR image shows a cystic lesion with thick walls, inner septa, and a solid nodule located in the right perirectum (*arrow*). A solid nodule is also seen anterior to the rectum (*arrowhead*). (**B**) PET-CT fused axial image shows elevated FDG uptake in the solid component of the right cystic lesion (*arrow*) and of the anterior perirectal nodule (*arrowhead*).

12. Subhas N, Patel PV, Pannu HK, et al. (2005) Imaging of pelvic malignancies with in-line FDG PET-CT: case examples and common pitfalls of FDG PET. Radiographics 25(4):1031–1043
13. Wahl RL (2004) Why nearly all PET of abdominal and pelvic cancers will be performed as PET/CT. J Nucl Med 45:82S–95S
14. Pannu HK, Cohade C, Bristow RE, et al. (2004) PET-CT detection of abdominal recurrence of ovarian cancer: radiologic-surgical correlation. Abdom Imaging 29(3):398–403
15. Dromain C, Leboulleux S, Auperin A, et al. (2008) Staging of peritoneal carcinomatosis: enhanced CT vs. PET/CT. Abdom Imaging 33:87–93
16. Suzuki A, Kawano T, Takahashi N, et al. (2004) Value of 18F-FDG PET in the detection of peritoneal carcinomatosis. Eur J Nucl Med Mol Imaging 31(10):1413–1420
17. Tanaka T, Kawai Y, Kanai M, et al. (2002) Usefulness of FDG-positron emission tomography in diagnostic peritoneal recurrence of colorectal cancer. Am J Surg 184:433–436
18. Turlakow A, Yeung HW, Salmon AS, Macapinlac HA, Larson SM (2003) Peritoneal carcinomatosis: role of (18)F-FDG PET. J Nucl Med 44(9):1407–1412
19. Meyers MA (2000) *Dynamic radiology of the abdomen. Normal and pathologic anatomy, 5th edition*. New York: Springer-Verlag

Fig. 19. Ovarian carcinoma—mesenteric neoplastic implant with bowel loop involvement. (**A**) Maximum-intensity projection FDG PET image shows a metabolically active mass in the lower abdomen. (**B**) Coronal fused PET-CT scan helps localize the increased activity seen at PET in the mesentery (*arrow*). (**C**) Axial contrast-enhanced CT shows parietal thickening of a bowel loop (*arrow*). (**D**) PET-CT fused axial scan discloses hypermetabolic activity of this bowel loop due to neoplastic involvement (*arrow*).

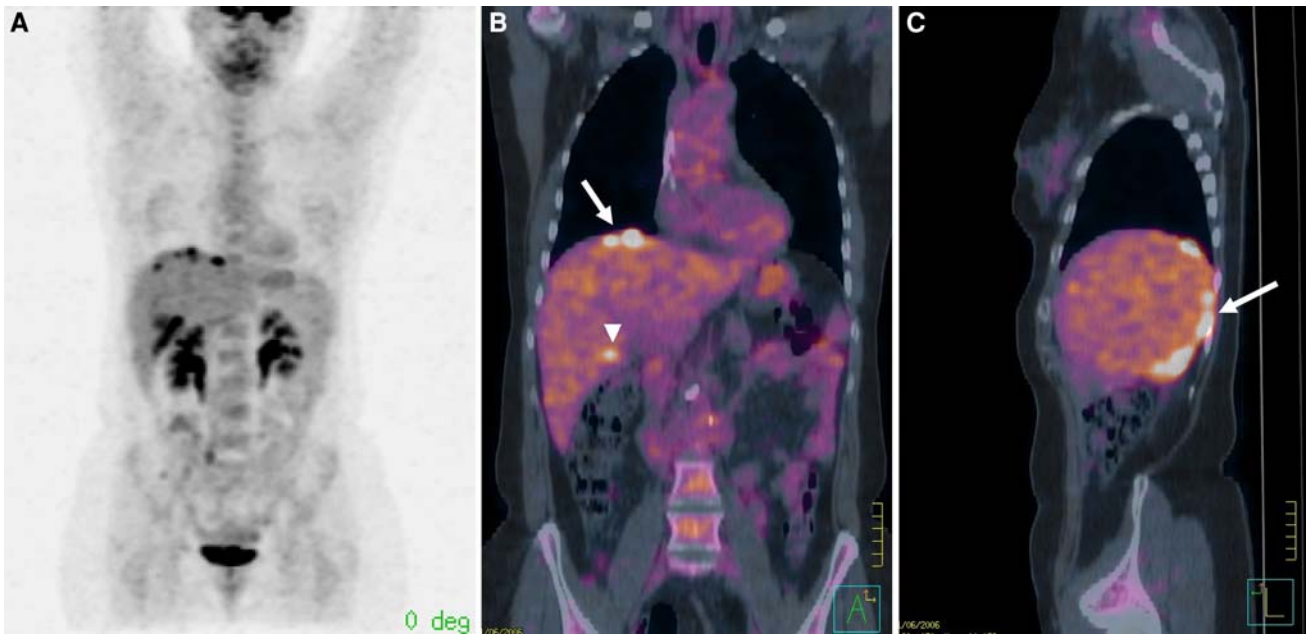

Fig. 20. Ovarian carcinoma—neoplastic implants over the liver capsule. (**A**) Maximum-intensity projection FDG PET image shows hypermetabolic tumor nodules over the dome, right lateral and posterior surface of the liver. Morison's pouch is also involved. The falciform and coronary ligaments prevent neoplastic diffusion to the left. (**B**) Coronal fused PET-CT scan shows nodules with high FDG uptake at the liver dome (*arrow*) and at the inferior surface of the right liver (*arrowhead*). (**C**) Sagittal fused PET-CT scan shows diffusion to the posterior surface of the right liver lobe.

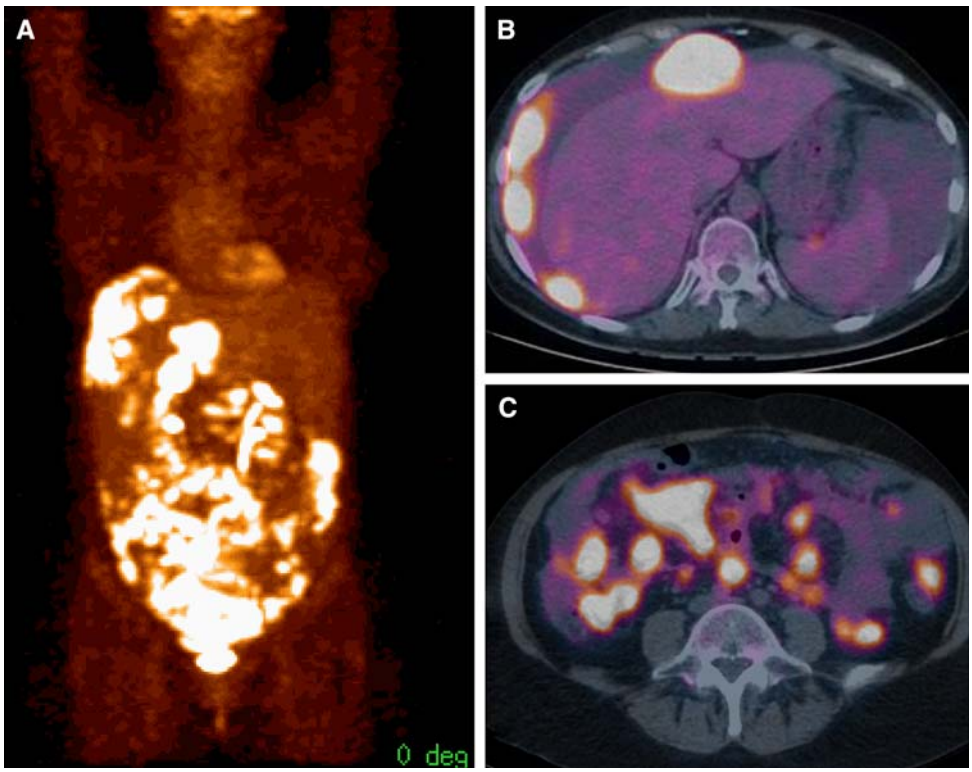

Fig. 21. Ovarian carcinoma—peritoneal carcinomatosis with ascites. (**A**) Maximum-intensity projection FDG PET image shows massive peritoneal involvement. (**B**) PET-CT fused axial scan discloses multiple nodules with high FDG uptake. The presence of ascites allows localization of the hypermetabolic foci in the parietal peritoneum. (**C**) Multiple foci of intense activity are also seen in the abdominal cavity among bowel loops.

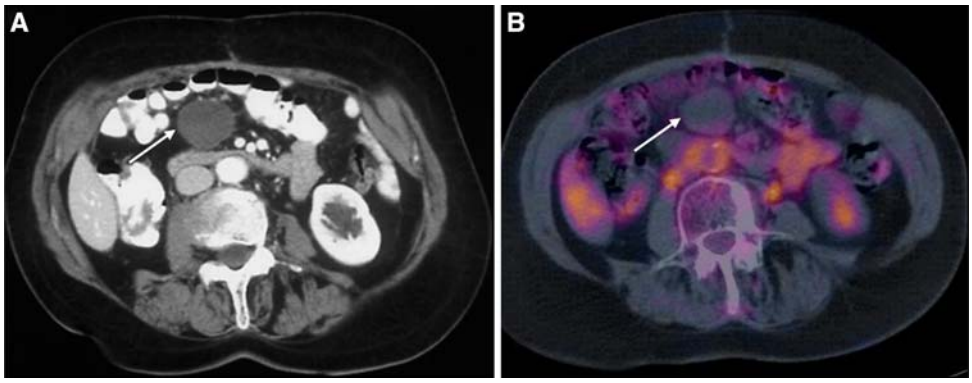

Fig. 22. Ovarian carcinoma cystic implant. (**A**) Axial postcontrast CT scan discloses a cystic lesion in the transverse mesocolon (*arrow*). (**B**) PET-CT fused axial scan shows no FDG uptake at the lesion site (*arrow*).

20. Meyers MA (1973) Distribution of intra-abdominal malignant seeding: dependency on dynamics of flow of ascitic fluid. Am J Roentgenol 119(1):198–206
21. DeMeo JH, Fulcher AS, Austin RF Jr (1995) Anatomic CT demonstration of the peritoneal spaces, ligaments, and mesenteries: normal and pathologic processes. RadioGraphics 15:755–770
22. Meyers MA, Oliphant M, Berne AS, Feldberg MA (1987) The peritoneal ligaments and mesenteries: pathways of intraabdominal spread of disease. Radiology 163(3):593–604
23. Meyers MA (1975) Metastatic seeding along small bowel mesentery: Roentgen features. Am J Roentgenol 123:67–73
24. Meyers MA (1995) Morison pouch. Radiology 195(2):578
25. Yoo E, Kim JH, Kim MJ, et al. (2007) Greater and lesser omenta: normal anatomy and pathologic processes. RadioGraphics 27:707–720
26. Dodiuk-Gad R, Ziv M, Loven D, et al. (2006) Sister Mary Joseph's nodule as a presenting sign of internal malignancy. Skinmed 5(5):256–258
27. Blake MA, Singh A, Setty BN, et al. (2006) Pearls and pitfalls in interpretation of abdominal and pelvic PET-CT. Radiographics 26(5):1335–1353

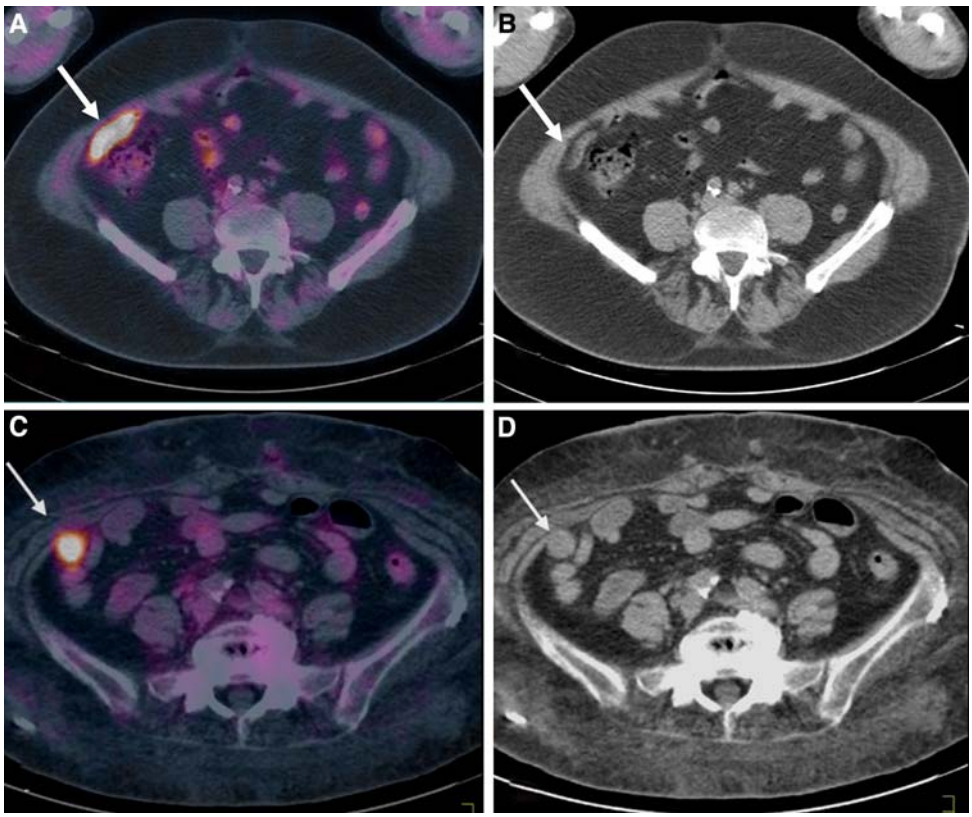

Fig. 23. Physiologic bowel uptake (**A** and **B**) versus neoplastic implant (**C** and **D**). (**A**) PET-CT fused axial scan shows focal FDG uptake in the right iliac fossa (*arrow*). (**B**) Low dose CT axial scan shows a normal appearing bowel loop at the site of FDG uptake (*arrow*). (**C**) PET-CT fused axial scan shows a focal area with intense FDG uptake in the right iliac fossa (*arrow*). (**D**) Low dose CT scan shows a soft tissue nodule adjacent to a bowel loop at the site of uptake (*arrow*). Laparoscopy confirmed neoplastic implants.

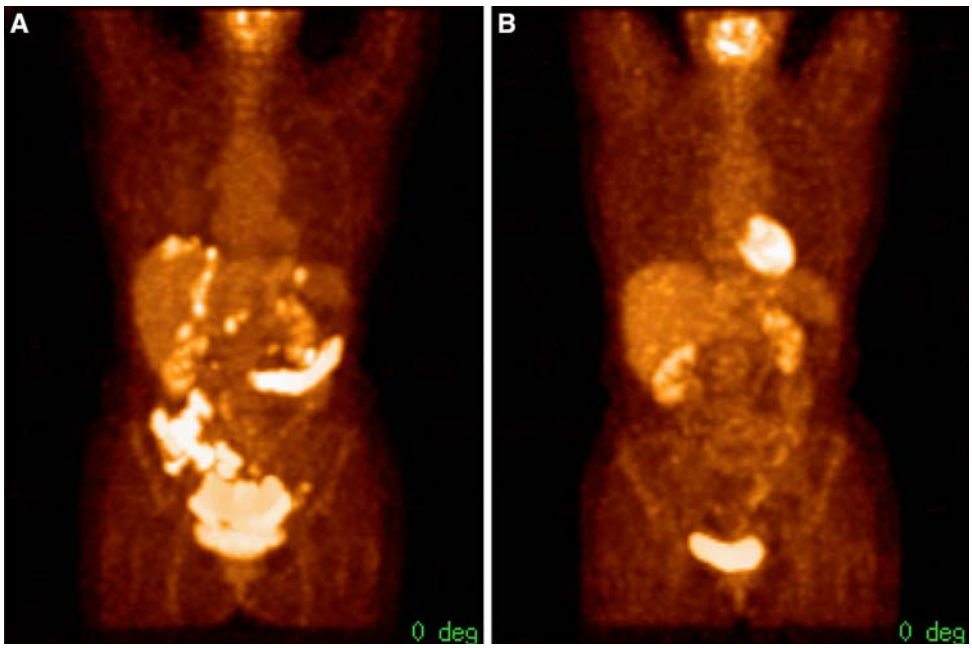

Fig. 24. Peritoneal carcinomatosis—diffuse peritoneal involvement. (**A**) Maximum-intensity projection PET image shows multiple areas of high FDG uptake in the abdomen and pelvis. Perihepatic diffusion and seeding along the falciform ligament are shown. (**B**) Post-chemotherapy evaluation: complete response was achieved and no focal area of increased FDG uptake is shown.